

Global climate forcing of aerosols tied to international trade

Jintai Lin^{1*†}, Dan Tong^{2†}, Steven Davis³, Ruijing Ni¹, Xiaoxiao Tan^{1,4}, Da Pan⁵, Hongyan Zhao², Zifeng Lu⁶, David Streets⁶, Tong Feng², Qiang Zhang^{2*}, Yingying Yan¹, Yongyun Hu¹, Jing Li¹, Zhu Liu⁷, Kebin He^{8,9}, Yi Huang^{4*}, Dabo Guan¹⁰

Affiliations:

¹ Laboratory for Climate and Ocean-Atmosphere Studies, Department of Atmospheric and Oceanic Sciences, School of Physics, Peking University, Beijing 100871, China.

² Ministry of Education Key Laboratory for Earth System Modeling, Center for Earth System Science, Tsinghua University, Beijing 100084, China.

³ Department of Earth System Science, University of California, Irvine, CA 92697, USA.

⁴ Department of Atmospheric & Oceanic Sciences, McGill University, Montreal, Quebec H3A 0B9, Canada.

⁵ Department of Civil and Environmental Engineering, Princeton University, Princeton, NJ 08544, USA.

⁶ Energy Systems Division, Argonne National Laboratory, Argonne, IL 60439, USA.

⁷ Resnick Sustainability Institute, California Institute of Technology, Pasadena, CA 91125, USA.

⁸ State Key Joint Laboratory of Environmental Simulation and Pollution Control, School of Environment, Tsinghua University, Beijing 100084, China.

⁹ Collaborative Innovation Center for Regional Environmental Quality, Beijing, 100084, China.

¹⁰ School of International Development, University of East Anglia, Norwich, NR4 7TJ, UK.

*Correspondence to: Jintai Lin (linjt@pku.edu.cn), Qiang Zhang (qiangzhang@mail.tsinghua.edu.cn), or Yi Huang (yi.huang@mcgill.ca)

† These authors contributed equally to this work.

Main Text:

4 pages of text (2454 words excluding references, acknowledgements and figure legends)

Figures 1-3

References: 1-31

Methods:

3158 words excluding references.

References: 32-101

Extended Data:

Extended Data Tables 1 and 2

Extended Data Figures 1-8

[Summary Paragraph]

International trade separates regions consuming goods and services from regions where goods and related aerosol pollution are produced¹. Yet the role of trade in aerosol climate forcing attributed to different regions has never been quantified. Here, we contrast the direct radiative forcing of aerosols related to regions' consumption of goods and services against the forcing due to emissions produced in each region. Aerosols assessed include black carbon, primary organic aerosol, and secondary inorganic aerosols including sulfate, nitrate and ammonium. We find that global aerosol radiative forcing due to emissions produced in East Asia is much stronger than the forcing related to goods and services ultimately consumed in that region because of its large net export of emissions-intensive goods. The opposite is true for net importers like Western Europe and North America: global radiative forcing related to consumption is much greater than the forcing due to emissions produced in these regions. Overall, trade is associated with a shift of radiative forcing from net importing to net exporting regions. Compared to greenhouse gases such as carbon dioxide, the short atmospheric lifetimes of aerosols cause large localized differences in radiative forcing. International efforts to reduce emissions in the exporters will help alleviate trade-related climate and health impacts of aerosols while lowering global emissions.

[210 words]

Anthropogenic aerosols influence the radiative balance of the climate system and constitute an important radiative forcing that drives global climate change²⁻⁶. Furthermore, the spatial pattern of aerosol forcing strongly affects regional climate⁷⁻¹³ – for example, Indian aerosols affect the summer monsoon precipitation^{9,13}, and Asian aerosols affect the Pacific storm track¹¹. Because aerosols stay in the atmosphere only for a few days, their effect on radiative forcing is most powerful around the regions where they or their precursor gases (from which these aerosols are formed) are emitted, with the potential for additional forcing due to aerosols transported to more distant areas by weather systems^{6-8,10,11}. Industrial processes and fossil fuel burning lead to emissions of aerosols and precursors as a byproduct, such that the emissions may be attributed to production of specific goods and services. In turn, international trade has increasingly enabled these production activities and their related aerosol emissions to occur far from where the goods and services are ultimately consumed. Accompanying the relocation of emissions is a change in the amount of emissions associated with a given product, as a result of regional differences in energy structure, energy efficiency, and emission control levels^{1,14}. Although the important role of international trade in redistributing carbon and pollutant emissions¹⁵⁻²² and altering regional air quality^{1,23} has been shown previously, the effects on climate forcing due to aerosols has never been assessed. Yet the potential implications for regional climate impacts are substantial, especially since aerosols are short-lived and exert strong spatially inhomogeneous forcing.

Here, we evaluate the role of trade in attributing top-of-the-atmosphere direct aerosol radiative forcing (RF) as of 2007, which is the most recent year for which all necessary data are available. As modeled, direct RF accounts for both scattering and absorption of solar radiation in the atmosphere, i.e., through aerosol-radiation interactions² (*Methods*). We quantify global direct RF related to aerosols produced in, as well as goods and services consumed in, each of 11 world regions: East Asia (China, Mongolia, and North Korea), Economies in Transition (Eastern Europe and Former Soviet Union), North America (the United States and Canada), Western Europe, Middle East and North Africa, Southeast Asia and Pacific, Pacific OECD (Japan, South Korea, Australia, and New Zealand), Latin America and Caribbean, South Asia, Sub-Saharan Africa, and Rest of the World (Extended Data Fig. 1).

We estimate global emissions of aerosols and precursors related to goods and services consumed in each region (consumption-based emissions, E_c) using a multi-regional input-output model based on trade data for 129 countries/regions and 57 industry sectors²⁴ and a newly built country- and sector-specific emission inventory of emissions produced within each region (production-based emissions, E_p) (*Methods*). Emitted species include nitrogen oxides (NO_x), sulfur dioxide (SO_2), ammonia (NH_3), carbon monoxide (CO), black carbon (BC), and primary organic aerosol (POA). Although it is not an aerosol precursor, CO is included due to its influence on the atmospheric oxidative capacity that affects the formation of secondary aerosols.

We then calculate production-based direct radiative forcing (RF_p) and consumption-based direct radiative forcing (RF_c) for each of the 11 regions

(*Methods*). We use the chemical transport model GEOS-Chem to simulate the atmospheric evolution of emitted BC and POA and secondary inorganic aerosols (SIOA, including sulfate, nitrate and ammonium) that are formed in the atmosphere from the emitted NO_x, SO₂ and NH₃ gases. Subsequently, we employ the radiative transfer model RRTMG to calculate the RF of BC, POA and SIOA. Cumulative global RF from included aerosols is about 0.32 W/m² for BC, -0.10 W/m² for POA, and -0.48 W/m² for SIOA, which are consistent with the mean values reported in the Intergovernmental Panel on Climate Change (IPCC) Fifth Assessment Report (AR5)² (0.40, -0.09, and -0.51 W/m² for aerosol-radiation interactions for BC, POA, and SIOA, respectively)². In magnitude, the RF of SIOA and BC is 18–26% of the RF of carbon dioxide (CO₂, 1.82 w/m²), and is comparable to the RF of methane (0.48 w/m²) and ozone (0.35 w/m²). Hereafter, we sum the negative RF of SIOA and POA.

Figure 1 shows regional differences in consumption- and production-based aerosol emissions (i.e. $E_c - E_p$), or the net emissions embodied in trade (emissions embodied in imports less emissions embodied in exports), for six aerosol and precursor species. Globally, 20% of NO_x emissions, 13% of CO, 26% of SO₂, 16% of NH₃, 11% of BC and 6% of POA in 2007 are related to production of goods and services that are consumed in a different region. Net exports are consistently largest for East Asia, representing about 20% of NO_x, SO₂, and NH₃ (5138, 7437, and 1765 Gg, respectively), 10% of BC (155 Gg), and 5% of POA (357 Gg) produced in the region, broadly consistent with previous estimates^{1,21}. Except for POA, these percentage differences exceed their associated uncertainties. For comparison, the emissions

exported on net from East Asia represent 47%, 121%, 46%, 46%, and 35% of the NO_x , SO_2 , NH_3 , BC, and POA produced in Western Europe, respectively. Net imports to Western Europe and North America embody the largest quantities of emissions, with consumption-based emissions, E_c , that exceed those regions' production-based emissions, E_p , by 39–120% in Western Europe and by 11–53% in North America (depending on the species). Overall, E_c of the developed (developing) countries are larger (lower) than their E_p , in line with previous emission studies^{15,20,22}.

Attributing emissions to the region where products are ultimately consumed means considerable re-attribution of RF at the regional scale. Extended Data Figs. 3 and 4 show the horizontal distributions of RF_p , RF_c and their differences for SIOA+POA and BC, respectively. The RF_p maps highlight the effect of atmospheric transport in transferring aerosols from the regions of emissions to downwind places, e.g., from East Asia to most regions in the Northern Hemisphere. The RF_c maps emphasize attribution of aerosol forcing related to regions' consumption by accounting for trade, e.g., from most regions to East Asia. Overall, trade-related relocation of production means that consumption in any region leads to aerosol forcing all over the world, to an extent much beyond the effect of atmospheric transport alone. Extended Data Fig. 5 further shows that although the positive forcing of BC largely compensates for the negative forcing of SIOA+POA on a global mean basis, regionally the locations of BC forcing do not always correlate to the locations of SIOA+POA forcing, leading to a clear spatial pattern of positive and negative forcing that affects the regional climate.

Figure 2 highlights the spatial distribution of the difference between RF_c and RF_p contributed by East Asia (first column), North America (second column) and Western Europe (third column). For East Asia, the magnitude of RF_c is larger than RF_p over the Southern Hemisphere, the Middle East and India, with stronger negative forcing of SIOA+POA (by up to -0.07 W/m^2) and stronger positive forcing of BC (by up to 0.04 W/m^2). This means that aerosol forcing due to emissions released in these regions associated with consumption in East Asia is stronger than the effect of atmospherically transported aerosols due to emissions released in East Asia. Over most of the Northern Hemisphere, the RF_c contributed by East Asia is weaker in magnitude than its RF_p . This is because the production-related aerosol concentrations greatly exceed concentrations of consumption-related aerosols over East Asia, and the atmospheric transport of excess production-related aerosols more than offsets the effect of trade-associated emission relocation.

For North America (Fig. 2, second column), the magnitude of RF_c exceeds its RF_p across most of the world. The difference is greatest over eastern China, with a peak value of -1.0 W/m^2 for SIOA+POA and 0.4 W/m^2 for BC. The negative values for SIOA+POA over western North America suggest that both eastern and western North America outsources production to East Asia, and the consequently enhanced atmospheric transport of East Asian aerosols more than offsets the effect of outsourcing-caused reduction in western North American emissions¹. This represents net transfer of aerosol RF from eastern to western North America. For Western Europe (Fig. 2, third column), the magnitude of RF_c is stronger than its RF_p

over most of the globe, with the largest differences over eastern China and the Middle East (by up to -0.7 W/m^2 for SIOA+POA and 0.4 W/m^2 for BC). Overall, we find that the combination of trade and atmospheric transport means effective globalization of aerosol RF associated with a given region's consumption.

Figure 3a and 3b summarizes the global average RF_c and RF_p contributed by individual regions. The magnitude of both RF_c and RF_p contributed by East Asia is the largest, followed by South Asia and Sub-Saharan Africa. Exports of these regions produce stronger aerosol forcing than their imports, and thus their RF_c are weaker in magnitude than RF_p , although the RF differences are often within the associated uncertainties for South Asia and Sub-Saharan Africa. In particular, the RF_c contributed by East Asia is -0.14 W/m^2 for SIOA+POA and 0.077 W/m^2 for BC, weaker than its RF_p at -0.17 and 0.085 W/m^2 , respectively. The RF_c versus RF_p differences, -0.03 W/m^2 for SIOA+POA and 0.008 W/m^2 for BC, are comparable to the absolute magnitude of RF_p contributed by Western Europe (for SIOA+POA) and North America (within 25% for both SIOA+POA and BC).

Figure 3a and 3b also shows that Western Europe, North America and Pacific OECD are net importers of goods, thus the radiative forcing related to their consumption, RF_c , is stronger than the forcing related to their produced emissions, RF_p , by 51–105% for SIOA+POA and by 69–94% for BC. A similar result is shown in Extended Data Fig. 6 for the net forcing of SIOA+POA+BC, although the cooling effect of SIOA+POA is largely offset by the warming effect of BC on a global mean basis.

For RF contributed by any given region, Fig. 3c and 3d depicts the percentage of forcing imposed upon the region's own territory, a metric to evaluate how much trade and atmospheric transport redistribute the aerosol RF. The territorial (domestic) percentage for RF_p ranges from 12% to 52% across all regions and species. In other words, for RF_p contributed by almost any given region, the forcing imposed outside the region's territory due to atmospheric transport is stronger than the forcing imposed upon its territory. This is because a large fraction of aerosols are transported away from the region's territory (Extended Data Fig. 7), and BC exerts enhanced RF per unit of mass when transported to higher altitudes³. For any given region and species, the territorial percentage for RF_c is always smaller than the percentage for RF_p . For Western Europe, the percentage for RF_c is 14% for SIOA+POA and 12% for BC, smaller than that for RF_p (30% and 22%, respectively) by a factor of two. For the Pacific OECD region, the percentage for RF_c is 8% for SIOA+POA and 9% for BC, smaller than that for RF_p (20% and 21%, respectively) by a factor of 2.5. These results suggest enhanced spatial spreading of consumption-associated aerosol RF via trade, in addition to the dispersion of emissions via atmospheric transport.

Our results show that a large portion of aerosol RF of East Asia is tied to consumption in the developed countries. This has an important effect on per capita RF. In particular, although aerosol RF_p per person in East Asia is larger than RF_p per person in North America and Western Europe (by 6–94% for SIOA+POA and 97–110% for BC, respectively), the sign of difference can be reversed when evaluated on

the basis of consumption (e.g., RF_c per capita of East Asia's SIOA+POA is weaker than North America by 43% and Western Europe by 23%) (Extended Data Fig. 8).

In addition to their direct RF quantified here, aerosols can affect cloud and precipitation processes and lead to indirect forcing on the regional and global climate^{2,9,13}. This indirect effect, although much harder to quantify due to current limitations in the understanding and modeling of the hydrological cycle², is also influenced by the proportion of a given region's consumption supplied via trade. Moreover, aerosols are harmful pollution to human health, causing more than three million premature deaths globally, including more than one million mortality in China in 2010²⁵. And trade is associated with a large quantity of deaths in regions supplying foreign consumption^{23,26}. For example, aerosol pollution associated with China's export causes an estimated 157,000 Chinese deaths in 2007²⁶, more than the deaths in the United States and the United Kingdom together from all ambient aerosol and ozone pollution in 2010²⁵. Thus, trade plays a critical role in connecting global production and consumption and associated pollutant emissions, health impacts and climate forcing.

The large aerosol direct RF contributed by East Asia and South Asia reflects these regions' fast growing economies, urbanization, coal-dominated energy sources, and relatively inefficient energy technologies and emission controls^{1,27}. Over the past decade, China—the largest emitter of aerosols and precursors in East Asia and the world—has made considerable progress in reducing its production-based emissions (E_p)—for example, SO_2 emissions from coal-fired power plants were halved from

2005 to 2010²⁸. Furthermore, China's CO₂ emission mitigation plan (i.e., Intended Nationally Determined Contribution²⁹) will have substantial co-benefits for reducing aerosol emissions by improving energy efficiency and boosting contribution from renewable energy sources. India has made similar pledges³⁰. Together these efforts will help to offset the effects of economic growth and increasing consumption on RF and human health, but the effects of trade highlighted by our analysis may partially counteract this progress if the long-term trend of offshoring production from Western Europe and North America to Asia³¹ persists. Thus, trade, environmental, and public health policies may be improved by explicitly considering the substantial geographical transfer of aerosol emissions and impacts related to international trade^{1,20,22}. Despite stringent policies in the developed countries, global emissions of many aerosol pollutants have increased in recent years, implying that efforts may need to be extended to consider emissions embodied in trade²⁰. To the extent these efforts seek to reduce the radiative forcing and health impacts of aerosols, mitigation of emissions in developing countries promises to be far less expensive than the incremental improvements in the relatively much-cleaner energy systems of the most-developed regions. For example, extension and revision of funding and technology transfer programs such as the Clean Development Mechanism developed under the Kyoto Protocol to include aerosol pollution might effectively reduce aerosol climate forcing and also help to improve air quality. Policymakers in developing countries might also consider the extent to which the costs of more stringent environmental regulations could be passed along to consumers in other regions. Our findings thus

suggest the possibility of analyses that compare the regional impacts of aerosols to the economic benefits of trade and the costs of improving production technologies.

Such analyses may serve as a scientific basis for political instruments addressing the trade-related environmental issues.

Methods

Five steps are taken to derive RF_p and RF_c of aerosols. The first step develops an inventory of anthropogenic emissions of SO_2 , NO_x , CO, BC, POA, and NH_3 produced in individual countries worldwide, i.e., a country-based E_p inventory. The inventory is built because existing global inventories (e.g. EDGAR and HTAP) lack detailed sectoral information necessary for tracing emissions through the global supply chain. The second step derives the global emissions related to goods and services ultimately consumed by individual countries, i.e., a country-based E_c inventory, by tracing goods and services through the global supply chain. The third step projects the country-based E_p and E_c inventories on a longitude-latitude grid to facilitate the subsequent atmospheric modeling. The fourth step employs a chemical transport model (CTM) to calculate to atmospheric evolution and transport of emitted species and secondary products they form, including SIOA. The gridded emissions are used to drive model simulations. The final step uses a radiative transfer model (RTM) to calculate the radiative forcing of aerosols, simulated by the CTM, related to production- or consumption-based emissions. The last two steps involve a series of CTM and RTM calculations to separate the RF of individual aerosols related to production or consumption of each of 11 aggregated regions. The 11 regions are chosen because of their geographic characteristics and economic and emission status (Fig S1).

Production-based emissions

Emissions of species other than NH_3

Production-based emissions represent pollutants physically released in each

region, and they are calculated as the product of emission factors and activity rates. A country-specific E_p inventory in 2007 for SO_2 , NO_x , CO, BC and POA is built for this study. The inventory uses a detailed technology-based methodology as in previous studies²⁻¹³, and it covers 65 sectors and 228 countries/regions worldwide. Global anthropogenic emissions in 2007 are estimated at 115.4 Tg for SO_2 , 112.9 Tg for NO_x , 534.0 Tg for CO, 6.0 Tg for BC, and 29.4 Tg for POA. [Here emitted POA is 2.1 times as much as organic carbon, after accounting for the oxygen atoms contained, consistent with the assumption in GEOS-Chem.] After the emission data are derived, they are further mapped to the 129 countries/regions and 57 sectors defined in the Global Trade Analysis Project version 8 (GTAP8)²⁴, in order to facilitate the subsequent calculation of consumption-based emissions. Emission factors and activity data are described as follows.

Activity data: We take the country-based fuel consumption data from the International Energy Agency (IEA)^{32,33} for 50 sub-sectors and 51 fuels in four major sectors (residential, industry, power, and transportation). We further aggregate these fuels into 20 types, considering that emissions related to certain fuels in the IEA database are small and their emission factors are not available^{27,34}. For Greenland, there are no fossil fuel data in the IEA database, thus we use the data compiled in the United States Energy Information Administration (<http://www.eia.gov/>). We then divide the fuel use in each sector by different technologies (four technologies in the power sector, 10 in industry, 21 in transportation, and 11 in the residential sector)³⁴⁻³⁷. The technology distributions for various vehicle types follow previous studies^{38,39}.

Biofuel combustion technologies in the residential sector follow the Greenhouse Gas and Air Pollution Interactions and Synergies (GAINS, <http://gains.iiasa.ac.at/models/>) model. In addition, we include 15 non-combustion industrial process sectors, taking production data from the United States Geological Survey statistics (USGS, <http://minerals.usgs.gov/minerals/pubs/myb.html>) and United Nations data (UNdata, <http://data.un.org/>).

Emission factors: We compile emission factors from a wide variety of literature and our previous works, including using data from reliable regional inventories to calibrate the emission factors for China, India, Southeast Asia, Canada, the United States, and Europe. Emission factors for SO₂ from fuel combustion follow our previous works^{27,40-43}. For the non-combustion sources, we take the unabated SO₂ emission factors from the public databases^{44,45}, and then we follow our previous studies^{27,37,41,42} to employ the flue gas desulfurization application rates and corresponding SO₂ removal efficiencies. We use regional emission inventories^{27,37,40,46,47} to calibrate the SO₂ emission factors for China, India, Southeast Asia, Canada, the United States, and Europe. Emission factors of NO_x and CO follow Yan et al.³⁹ for on-road vehicles and several public databases^{44,45,48} for other sources; we further replace the global defaults by regional emission databases where available^{35,49-53}. For BC and POA, we take the emission factors from Bond et al.^{34,54}, except that we follow Yan et al.^{38,39} for on-road vehicles, Lam et al.⁵⁵ and Huang et al.⁵⁶ for residential kerosene, and our previous works^{27,46} for all emission factors of China and India.

Emissions of NH₃

An additional country-based E_p data base is built here for NH₃ in 2007.

Emissions are calculated for 129 countries/regions and 57 sectors (13 for agricultural activities) defined in GTAP8²⁴. We combine the global EDGAR inventory and several existing regional inventories that often have more detailed sectoral information to facilitate a global supply chain analysis (see Extended Data Table 2). For example, although agriculture accounts for 96% of global anthropogenic NH₃ emissions, there are 2–3 agricultural sectors only in EDGAR and other global inventories, whereas much more information is available in the regional inventories for the United States, China, and Europe. For regions other than the United States, China and Europe, agricultural emissions are often sorted in the inventories according to sources (e.g. fertilizer, compost, and manure) instead of sectors. In this case, we map the source-based emissions to individual agricultural sectors, using as weighting functions the regionally aggregated (over regions other than China, the US, and Europe) contributions of individual agricultural sectors from MASAGE.

Comparison with HTAP v2

The scatterplot in Fig. S2 compares the E_p inventory built here with the HTAP v2 inventory for 2008⁵⁷. HTAP v2 was recently developed from an internationally collaborative project, and it combines the EDGAR inventory⁵⁸ with regional inventories in Asia, North America, and Europe. HTAP v2 is thus expected to be more updated than EDGAR and other older global inventories. Figure S2 shows that total E_p emissions in our inventory are in line with HTAP v2. Our inventory is

spatially consistent with HTAP v2 with a correlation coefficient of 0.99–1.00 for all the six species. The bias relative to HTAP v2 is within 8% for NO_x, CO, SO₂ and NH₃, 11% for BC, and 18% for POA. The differences for China, India, the United States and other large emitters are generally small. Although the differences are larger for small emitters, as expected, they are normally within the uncertainty of current emission inventories^{3,59}.

Consumption-based emissions

Consumption-based emissions represent pollutants released along the global supply chain as a result of certain region's consumption of final products and services. For example, a cell phone purchased in the United States may be assembled in China with iron ores mined in Australia, Steel made in Japan and high-end assembling mechanics manufactured in the United States. And consumption-based emissions attribute the pollutants consequently released in these countries to the United States.

Here we use the multi-regional input-output model (MRIO) from GTAP8²⁴, based on monetary flows, to trace the economic interconnections among sectors and regions. We then combine the MRIO analysis with the production-based emission inventory to obtain the consumption-based emissions on a country and sectoral basis. The above method has been used to calculate consumption-based emissions of CO₂ and air pollutants^{15,20,21,60,61}, and used to evaluate export-related environmental and health impact^{1,26}. Detailed descriptions of the MRIO approach are provided in previous studies^{18,21,60}. Below is a brief introduction of this approach.

$$\mathbf{x} = \mathbf{Ax} + \mathbf{y} = (\mathbf{I} - \mathbf{A})^{-1}\mathbf{y} \quad (1)$$

$$\mathbf{E}' = \hat{\mathbf{f}}(\mathbf{I} - \mathbf{A})^{-1}\mathbf{y}' \quad (2)$$

Equation 1 shows how final consumption is supplied through the supply chain across 129 countries and 57 sectors. Here \mathbf{x} is a vector for country- and sector-specific monetary outputs to supply the associated final consumption \mathbf{y} (e.g., supplied by any given country and sector to all countries and sectors), \mathbf{Ax} is the intermediate outputs, $(\mathbf{I} - \mathbf{A})^{-1}$ is the Leontief inverse matrix, \mathbf{A} is the direct requirement coefficient matrix, and \mathbf{I} is the unit matrix. Equation 2 calculates region- and sector-specific consumption-based emissions \mathbf{E}' associated with final consumption \mathbf{y}' (e.g., supplied by all countries and sectors to any given country and sector). Here $\hat{\mathbf{f}}$ is the diagonalization of a vector representing region- and sector-explicit emissions per monetary output, as derived by dividing production-based emissions by monetary outputs \mathbf{x} . Values of \mathbf{y} , \mathbf{y}' and \mathbf{A} are available in the MRIO model, and region- and sector-explicit production-based emissions are derived in this study.

Gridded monthly emissions

Gridded emissions are required to drive the chemical transport modeling. We convert the country-based annual emissions to a monthly 0.1° long. x 0.1° lat. gridded dataset, based on the horizontal and monthly distribution of the HTAP v2 emission inventory for 2008⁵⁷. To support the atmospheric simulations, in the model world, E_c of any region is released in countries producing goods to supply that region – for example, a portion of China’s emissions is related to consumption in North America,

and in simulating the effect of E_c of North America, this portion is released within the Chinese territory and is gridded following China's E_p .

Prior to the conversion, we map our emissions from 57 sectors to five main sectors designated in HTAP v2 (power generation, industry, transportation, residential use, and agriculture).

Atmospheric evolution and transport simulated by GEOS-Chem

We use the global GEOS-Chem CTM version 9-02 to simulate the atmospheric evolution of aerosols and precursor gases. A series of model simulations are conducted to derive the individual effects of E_p and E_c of the 11 aggregated regions on the atmospheric distribution of SIOA, POA and BC.

GEOS-Chem is driven by the GEOS-5 assimilated meteorology from the NASA Global Modeling and Assimilation Office (GMAO). The model is run on a 2.5° long. x 2° lat. grid with 47 vertical layers, with full O_x - NO_x -VOC-CO- HO_x gaseous chemistry^{62,63} and online aerosol calculations. Simulated aerosols include SIOA^{64,65}, POA, BC^{65,66}, dust^{67,68}, and sea salts^{69,70}. POA is simulated as primary organic carbon with halved mass to account for the oxygen molecules contained⁷¹. SIOA is assumed to be in thermodynamical equilibrium following ISOROPIA-II⁷². Wet scavenging of soluble aerosols and gases in convective updrafts, rainout, and washout follows Liu et al.⁷³, with updates for BC by Wang et al.⁷⁴. Dry deposition of gases and aerosols follow Wesely⁷⁵ and Zhang et al.⁷⁶, respectively. Model advection uses the TPCORE algorithm of Lin and Rood⁷⁷, convection follows a modified Relaxed Arakawa-Schubert scheme⁷⁸, and mixing in the boundary layer follows a non-local scheme^{79,80}.

Global anthropogenic emissions of NO_x, SO₂, NH₃, CO, BC and POA are derived in this study. Other emissions are set as follows. Global anthropogenic emissions of non-methane volatile organic compounds (NMVOC) are taken from the RETRO dataset for 2000 as described by Hu et al.⁸¹; emissions in China, the rest of Asia and the United States are further replaced by the regional inventories MEIC for 2008 (www.meicmodel.org), INTEX-B for 2006³⁵ and NEI05 for 2005 (ftp://aftp.fsl.noaa.gov/divisions/taq/emissions_data_2005), respectively. Biogenic emissions of NMVOC follow the MEGAN model⁸². Soil emissions of NO_x follow Hudman et al.⁸³. Lightning emissions of NO_x follow the Price and Rind scheme with a satellite-based adjustment and a backward 'C-shape' vertical profile⁸⁴⁻⁸⁶. Biomass burning emissions use the monthly GFED-3 data for 2007⁸⁷.

We conduct three sets of model simulations for 2007 with a spin-up period of 6 months. The first set contains a control simulation (S1) with all emissions unperturbed and a second simulation (S2) with anthropogenic emissions of NO_x, SO₂, NH₃, CO, BC and POA removed globally. The second set of simulations (S3 to S13) tests the contributions of production-based emissions from the 11 regions, by removing anthropogenic emissions produced within their territories, one region at a time. The third set of simulations (S14 to S24) is the counterpart of the second set. It turns off global anthropogenic emissions related to consumption of each of these 11 regions. For each simulation, GEOS-Chem outputs 3-hourly 3-dimensional mass concentrations of SIOA, POA and BC for further radiative forcing calculations.

Radiative forcing calculations using RRTMG

We use the RRTMG RTM for shortwave (RRTMG_SW version v3.9)⁸⁸ to calculate the all-sky top-of-the-atmosphere RF of SIOA, POA and BC, based on the atmospheric distributions of aerosols simulated by GEOS-Chem. The RF accounts for scattering and absorption of solar radiation in the atmosphere, i.e., the RF from aerosol-radiation interactions. It does not account for rapid adjustments or feedbacks of clouds and the hydrological cycle. The longwave RF is negligible⁷¹ and not calculated here. Aerosols are assumed to mix externally to facilitate a species-specific RF calculation, and each aerosol type has a prescribed dry size distribution. Aerosol microphysical properties follow Heald et al.⁷¹, including dry size distributions, hygroscopic growth factors, and refractive indices. Following Hansen et al.⁴, we further scale the RF of BC by a factor of two to account for enhanced absorption by internal mixing with other aerosols³⁻⁵.

The spatially and temporally varying aerosol mass concentrations are obtained from the GEOS-Chem outputs. Ancillary meteorological and surface albedo data are taken from the GEOS-5 dataset, including cloud fraction, liquid water content, ice water content, air temperature, relative humidity, tropopause pressure, and air pressure profiles. The effective droplet radius is assumed as 14.2 μm for liquid clouds and 24.8 μm for ice clouds⁷¹.

Three sets of RTM calculations, with a total of 70 runs, are conducted for 2007 in correspondence to the sets of CTM simulations. The first set contains a run (R1) including all anthropogenic aerosols globally and three subsequent runs (R2–R4) that

are similar to R1 but removing global anthropogenic SIOA, POA and BC one by one. The second and third sets contain 33 (3 species x 11 regions per species) runs each, in which an aerosol species related to a given region's production or consumption is removed. To reduce the computational costs, the 3-hourly CTM aerosol data are averaged for each month to produce monthly mean 3-hourly datasets (i.e., the monthly mean diurnal cycle is preserved). The difference in RF between this monthly-mean based calculation and a calculation based on daily data is very small, according to our initial test.

The change from R_i ($i = 2$ to 70) to R_1 gives the RF of an aerosol species globally ($i = 2$ to 4), related to a region's production (RF_p , $i = 5$ to 37), or related to a region's consumption (RF_c , $i = 38$ to 70). For any aerosols (SIOA, POA and BC), the globally cumulated RF responds quite linearly to emission perturbations, as revealed by the fact that the RF_c is the same as the RF_p if the contributions of all regions are summed (Extended Data Table 1). The RF of SIOA contributed by individual regions may respond more nonlinearly to emission perturbations due to changes in the atmospheric oxidative capacity, dependence of sulfate and nitrate formation on the amount of NH_3 ⁸⁹, and additional nonlinearity in radiative transfer calculation. This nonlinearity is reduced here since emissions of all species are perturbed simultaneously in the CTM simulations, including CO that affects the oxidative capacity.

Uncertainties and limitations

Our estimated global RF_p and RF_c (summed across the contributions of all regions) are both about 0.32 w/m^2 for BC, -0.10 w/m^2 for POA, and -0.48 w/m^2 for SIOA, comparable to the mean values estimated in the IPCC AR5 (0.40 w/m^2 , -0.09 w/m^2 and -0.51 w/m^2 , respectively)². [Note that although the IPCC AR5 values are for the anthropogenic aerosol changes from 1750 to 2011, the anthropogenic emissions are negligible in 1750^{71,90}, and the changes from 2007 to 2011 are very small².] Here we provide a general discussion of errors in emissions, CTM and RTM relevant to the global and regional RF and the relative difference between regional RF_c and RF_p . All errors are referred to as 2σ uncertainties that correspond to a 95% confidence interval.

The calculation of E_p is subject to errors in national production data and emission factors^{1,14,58}. The HTAP assessment report⁸⁹ suggests a lower bound of errors in the global total E_p to be 10–30% for the species studied here. Regionally, E_p may contain larger errors in the developing countries due to less accurate data inputs; this additional error is estimated here to be within 30%, by comparing E_p for the 11 individual regions between the HTAP v2 inventory and our results.

Regionally, E_c shares most errors with E_p , although E_c contains an additional error from the MRIO calculation^{1,18} associated with inaccuracies in national economic statistics, sectoral details and data harmonization^{91,92}. Peters et al.³¹ showed that regional E_p and E_c of CO_2 have comparable variability across studies that use different MRIO models, suggesting a very small MRIO-related error compared to the error in

E_p . The study on China's trade with a detailed statistical analysis by Lin et al.¹ showed that the uncertainty in the input-output analysis contributes ~ 10% of total errors in export-related emissions of pollutants, with the remaining 90% from the calculation of E_p . Considering the MRIO-related error, here we assume a 10% additive error for E_c on top of the error translated from E_p . This leads to the error values (2σ) presented in Fig. 1.

Given the amount of emissions, the RF calculation is subject to errors in the CTM-simulated atmospheric processes^{63,89} and the RTM-simulated radiative transfer processes. The atmospheric loadings and vertical profiles of aerosols are relatively well simulated by the CTM here^{71,93}. Larger uncertainties exist in the current understanding of aerosol optical properties^{3,4,71}, such as the extent of absorption enhancement of BC through internal mixing³ and the absorption capability of POA⁹⁴. The CTM and RTM related errors together are on the order of 30% for SIOA, 50% for POA, and 100% for BC^{3,71,93,95}.

It is computationally prohibitive to perform systematic Monte Carlo or sensitivity analyses that integrate all errors associated with emissions, CTM and RTM. Here we give a rough estimate. Globally accumulated RF_p and RF_c share the same errors, and we estimate an error of 40% for SIOA, 60% for POA, and 150% for BC (i.e., by a factor of 2.5), based on the uncertainties adopted in the IPCC AR5². The errors for regional RF_p and RF_c may be larger for less-studied developing regions. Nevertheless, most errors in regional RF_p and RF_c are common and do not affect their relative difference¹, except for the effect of MRIO-related error on RF_c (inherited

from E_c). To account for the MRIO-related error, we assume a 10% additive error for regional RF_c on top of the error translated from RF_p . This leads to the error values (2σ) presented in Fig. 3.

Due to lack of data, we do not consider the impact of trade on aerosols related to international aviation or shipping. Nor do we include secondary organic aerosols because of considerable difficulties and uncertainties in emission calculations and chemical simulations. Although some portions of POA may absorb the solar radiation and partly (by 27%) offset the negative RF by POA scattering⁹⁴, we do not account for this absorption due to large uncertainties in determining the absorbing POA, consistent with the IPCC AR5 assumption. We also do not quantify the indirect RF of aerosols. Inclusion of these aspects would reveal additional effects of trade on aerosol RF.

References:

- 1 Lin, J.-T. *et al.* China's international trade and air pollution in the United States. *Proceedings of the National Academy of Sciences* **111**, 1736-1741, doi:10.1073/pnas.1312860111 (2014).
- 2 Myhre, G., D. Shindell, F.-M. Bréon, W. Collins, J. Fuglestedt, J. Huang, D. Koch, J.-F. Lamarque, D. Lee, B. Mendoza, T. Nakajima, A. Robock, G. Stephens, T. Takemura, H. Zhang. in *Climate Change 2013: The Physical Science Basis. Contribution of Working Group I to the Fifth Assessment Report of the Intergovernmental Panel on Climate Change* (ed T.F. Stocker, D. Qin, G.-K. Plattner, M. Tignor, S.K. Allen, J. Boschung, A.

- Nauels, Y. Xia, V. Bex and P.M. Midgley) (2013).
- 3 Bond, T. C. *et al.* Bounding the role of black carbon in the climate system: A scientific assessment. *Journal of Geophysical Research* **118**, 5380-5552 (2013).
- 4 Hansen, J. *et al.* Efficacy of climate forcings. *Journal of Geophysical Research: Atmospheres (1984–2012)* **110** (2005).
- 5 Jacobson, M. Z. Strong radiative heating due to the mixing state of black carbon in atmospheric aerosols. *Nature* **409**, 695-697 (2001).
- 6 Ramanathan, V. & Carmichael, G. Global and regional climate changes due to black carbon. *Nature Geoscience* **1**, 221-227 (2008).
- 7 Ruckstuhl, C. *et al.* Aerosol and cloud effects on solar brightening and the recent rapid warming. *Geophysical Research Letters* **35** (2008).
- 8 Shindell, D. & Faluvegi, G. Climate response to regional radiative forcing during the twentieth century. *Nature Geoscience* **2**, 294-300 (2009).
- 9 Bollasina, M. A., Ming, Y. & Ramaswamy, V. Anthropogenic aerosols and the weakening of the South Asian summer monsoon. *Science* **334**, 502-505 (2011).
- 10 Leibensperger, E. *et al.* Climatic effects of 1950–2050 changes in US anthropogenic aerosols—Part 2: Climate response. *Atmospheric Chemistry and Physics* **12**, 3349-3362 (2012).
- 11 Wang, Y. *et al.* Assessing the effects of anthropogenic aerosols on Pacific storm track using a multiscale global climate model. *Proceedings of the*

- National Academy of Sciences* **111**, 6894-6899 (2014).
- 12 Fiore, A. M. *et al.* Global air quality and climate. *Chemical Society Reviews* **41**, 6663-6683, doi:10.1039/c2cs35095e (2012).
- 13 Lau, K. M. & Kim, K. M. Observational relationships between aerosol and Asian monsoon rainfall, and circulation. *Geophysical Research Letters* **33** (2006).
- 14 Liu, Z. *et al.* Reduced carbon emission estimates from fossil fuel combustion and cement production in China. *Nature* **524**, 335-338, doi:10.1038/nature14677 (2015).
- 15 Moran, D. D., Lenzen, M., Kanemoto, K. & Geschke, A. Does ecologically unequal exchange occur? *Ecological Economics* **89**, 177-186 (2013).
- 16 Blanco G., R. G., S. Suh, J. Barrett, H. C. de Coninck, C. F. Diaz Morejon, R. Mathur, N. Nakicenovic, A. Ofori Ahenkora, J. Pan, H. Pathak, J. Rice, R. Richels, S. J. Smith, D. I. Stern, F. L. Toth, and P. Zhou, 2014. in *Climate Change 2014: Mitigation of Climate Change. Contribution of Working Group III to the Fifth Assessment Report of the Intergovernmental Panel on Climate Change* (ed O. Edenhofer, R. Pichs-Madruga, Y. Sokona, E. Farahani, S. Kadner, K. Seyboth, A. Adler, I. Baum, S. Brunner, P. Eickemeier, B. Kriemann, J. Savolainen, S. Schlömer, C. von Stechow, T. Zwickel, J.C. Minx) (2014).
- 17 Guan, D. *et al.* The socioeconomic drivers of China's primary PM_{2.5} emissions. *Environmental Research Letters* **9**, 024010 (2014).

- 18 Peters, G. P., Minx, J. C., Weber, C. L. & Edenhofer, O. Growth in emission transfers via international trade from 1990 to 2008. *Proceedings of the National Academy of Sciences* **108**, 8903 (2011).
- 19 Weber, C. L. & Matthews, H. S. Embodied environmental emissions in US international trade, 1997-2004. *Environmental Science & Technology* **41**, 4875-4881, doi:10.1021/es0629110 (2007).
- 20 Kanemoto, K., Moran, D., Lenzen, M. & Geschke, A. International trade undermines national emission reduction targets: New evidence from air pollution. *Global Environmental Change* **24**, 52-59 (2014).
- 21 Zhao, H. Y. *et al.* Assessment of China's virtual air pollution transport embodied in trade by using a consumption-based emission inventory. *Atmos. Chem. Phys.* **15**, 5443-5456, doi:10.5194/acp-15-5443-2015 (2015).
- 22 Oita, A. *et al.* Substantial nitrogen pollution embodied in international trade. *Nature Geoscience* **9**, 111-115, doi:10.1038/ngeo2635 (2016).
- 23 Takahashi, K. *et al.* Production-based emissions, consumption-based emissions and consumption-based health impacts of PM 2.5 carbonaceous aerosols in Asia. *Atmospheric Environment* **97**, 406-415 (2014).
- 24 Narayanan, G. B., Aguiar, A. & McDougall, R. Global Trade, Assistance, and Production: The GTAP 8 Data Base. (Center for Global Trade Analysis, Purdue University, West Lafayette, Indiana, 2012).
- 25 Lim, S. S. *et al.* A comparative risk assessment of burden of disease and injury attributable to 67 risk factors and risk factor clusters in 21 regions, 1990 –

- 2010: a systematic analysis for the Global Burden of Disease Study 2010. *Lancet* **380**, 2224-2260 (2012).
- 26 Jiang, X. *et al.* Revealing the hidden health costs embodied in Chinese exports. *Environmental Science & Technology*, doi:10.1021/es506121s (2015).
- 27 Lu, Z., Zhang, Q. & Streets, D. G. Sulfur dioxide and primary carbonaceous aerosol emissions in China and India, 1996–2010. *Atmos. Chem. Phys* **11**, 9839-9864 (2011).
- 28 Zhang, Q., He, K. B. & Huo, H. Cleaning China's air. *Nature* **484**, 161-162 (2012).
- 29 China. ENHANCED ACTIONS ON CLIMATE CHANGE: CHINA'S INTENDED NATIONALLY DETERMINED CONTRIBUTIONS. (Department of Climate Change, National Development & Reform Commission of China, Beijing, 2015).
- 30 India. INDIA'S INTENDED NATIONALLY DETERMINED CONTRIBUTION: WORKING TOWARDS CLIMATE JUSTICE. (2015).
- 31 Peters, G., Davis, S. & Andrew, R. A synthesis of carbon in international trade. *Biogeosciences* **9** (2012).
- 32 IEA. *Energy statistics and balances of OECD countries, 2007-2008* (International Energy Agency, 2010).
- 33 IEA. *Energy statistics and balances of Non-OECD countries, 2007-2008* (International Energy Agency, 2010).
- 34 Bond, T. C. *et al.* A technology-based global inventory of black and organic

- carbon emissions from combustion. *J. Geophys. Res.* **109** (2004).
- 35 Zhang, Q. *et al.* Asian emissions in 2006 for the NASA INTEX-B mission. *Atmospheric Chemistry and Physics* **9**, 5131-5153 (2009).
- 36 Streets, D. *et al.* An inventory of gaseous and primary aerosol emissions in Asia in the year 2000. *J. Geophys. Res.* **108**, 8809 (2003).
- 37 Liu, F. *et al.* High-resolution inventory of technologies, activities, and emissions of coal-fired power plants in China from 1990 to 2010. *Atmospheric Chemistry and Physics* **15**, 13299-13317, doi:10.5194/acp-15-13299-2015 (2015).
- 38 Yan, F., Winijkul, E., Jung, S., Bond, T. C. & Streets, D. G. Global emission projections of particulate matter (PM): I. Exhaust emissions from on-road vehicles. *Atmospheric Environment* **45**, 4830-4844, doi:10.1016/j.atmosenv.2011.06.018 (2011).
- 39 Yan, F. *et al.* Global emission projections for the transportation sector using dynamic technology modeling. *Atmospheric Chemistry and Physics* **14**, 5709-5733, doi:10.5194/acp-14-5709-2014 (2014).
- 40 Lu, Z. *et al.* Sulfur dioxide emissions in China and sulfur trends in East Asia since 2000. *Atmospheric Chemistry and Physics* **10**, 6311-6331, doi:10.5194/acp-10-6311-2010 (2010).
- 41 Streets, D. G., Wu, Y. & Chin, M. Two-decadal aerosol trends as a likely explanation of the global dimming/brightening transition. *Geophysical Research Letters* **33**, 4, doi:10.1029/2006gl026471 (2006).

- 42 Streets, D. G. *et al.* Anthropogenic and natural contributions to regional trends in aerosol optical depth, 1980-2006. *Journal of Geophysical Research-Atmospheres* **114**, 16, doi:10.1029/2008jd011624 (2009).
- 43 Streets, D. G. *et al.* Aerosol trends over China, 1980-2000. *Atmospheric Research* **88**, 174-182, doi:10.1016/j.atmosres.2007.10.016 (2008).
- 44 EMEP. EMEP/EEA air pollutant emission inventory guidebook 2013: Technical guidance to prepare national emission inventories. (2013).
- 45 USEPA. Compilation of Air Pollutant Emission Factors (AP-42). U.S. Environmental Protection Agency. (1999).
- 46 Lei, Y., Zhang, Q., He, K. B. & Streets, D. G. Primary anthropogenic aerosol emission trends for China, 1990-2005. *Atmospheric Chemistry and Physics* **11**, 931-954, doi:10.5194/acp-11-931-2011 (2011).
- 47 Lu, Z. & Streets, D. G. The Southeast Asia Composition, Cloud, Climate Coupling Regional Study Emission Inventory, available at: <http://bio.cgrer.uiowa.edu/SEAC4RS/emission.html> (last access: 26 March 2014), (2012).
- 48 Olivier, J. *et al.* Applications of EDGAR Emission Database for Global Atmospheric Research. *Rijksinstituut Voor Volksgezondheid En Milieu Rivm* (2002).
- 49 Zhang, Q. *et al.* NO_x emission trends for China, 1995–2004: The view from the ground and the view from space. *J. Geophys. Res* **112**, D22306 (2007).
- 50 Kurokawa, J. *et al.* Emissions of air pollutants and greenhouse gases over

- Asian regions during 2000–2008: Regional Emission inventory in ASia (REAS) version 2. *Atmos. Chem. Phys.* **13**, 11019-11058 (2013).
- 51 Lu, Z. F. & Streets, D. G. Increase in NO_x Emissions from Indian Thermal Power Plants during 1996-2010: Unit-Based Inventories and Multisatellite Observations. *Environmental Science & Technology* **46**, 7463-7470, doi:10.1021/es300831w (2012).
- 52 Vestreng, V. *et al.* Evolution of NO_x emissions in Europe with focus on road transport control measures. *Atmospheric Chemistry and Physics* **9**, 1503-1520, doi:10.5194/acp-9-1503-2009 (2009).
- 53 Yevich, R. & Logan, J. A. An assessment of biofuel use and burning of agricultural waste in the developing world. *Global Biogeochemical Cycles* **17**, 42, doi:10.1029/2002gb001952 (2003).
- 54 Bond, T. C. *et al.* Historical emissions of black and organic carbon aerosol from energy-related combustion, 1850-2000. *Global Biogeochemical Cycles* **21**, Gb2018, doi:10.1029/2006gb002840 (2007).
- 55 Lam, N. L. *et al.* Household Light Makes Global Heat: High Black Carbon Emissions From Kerosene Wick Lamps. *Environmental Science & Technology* **46**, 13531-13538, doi:10.1021/es302697h (2012).
- 56 Huang, Y. *et al.* Global organic carbon emissions from primary sources from 1960 to 2009. *Atmospheric Environment* **122**, 505-512, doi:10.1016/j.atmosenv.2015.10.017 (2015).
- 57 Janssens-Maenhout, G. *et al.* HTAP_v2.2: a mosaic of regional and global

- emission gridmaps for 2008 and 2010 to study hemispheric transport of air pollution. *Atmospheric Chemistry & Physics* **15**, 12867-12909 (2015).
- 58 Janssens-Maenhout, G., Petrescu, A. M. R., Muntean, M. & Blujdea, V. *Verifying Greenhouse Gas Emissions: Methods to Support International Climate Agreements*. (The National Academies Press, 2010).
- 59 Janssens-Maenhout, G. *et al.* *EDGAR-HTAP: a harmonized gridded air pollution emission dataset based on national inventories*. (Publications Office, 2011).
- 60 Davis, S. J. & Caldeira, K. Consumption-based accounting of CO₂ emissions. *Proceedings of the National Academy of Sciences of the United States of America* **107**, 5687-5692, doi:10.1073/pnas.0906974107 (2010).
- 61 Feng, K. *et al.* Outsourcing CO₂ within China. *Proc. Natl Acad. Sci. USA* **110**, 11654-11659 (2013).
- 62 Mao, J. *et al.* Ozone and organic nitrates over the eastern United States: Sensitivity to isoprene chemistry. *Journal of Geophysical Research: Atmospheres* **118**, 11,256-211,268, doi:10.1002/jgrd.50817 (2013).
- 63 Yan, Y.-Y., Lin, J.-T., Chen, J. & Hu, L. Improved simulation of tropospheric ozone by a global-multi-regional two-way coupling model system. *Atmos. Chem. Phys.* **16**, 2381-2400, doi:10.5194/acp-16-2381-2016 (2016).
- 64 Park, R. J., Jacob, D. J., Field, B. D., Yantosca, R. M. & Chin, M. Natural and transboundary pollution influences on sulfate-nitrate-ammonium aerosols in the United States: Implications for policy. *Journal of Geophysical Research-*

- Atmospheres* **109**, D15204, doi:10.1029/2003jd004473 (2004).
- 65 Park, R. J., Jacob, D. J., Kumar, N. & Yantosca, R. M. Regional visibility statistics in the United States: Natural and transboundary pollution influences, and implications for the Regional Haze Rule. *Atmospheric Environment* **40**, 5405-5423, doi:10.1016/j.atmosenv.2006.04.059 (2006).
- 66 Park, R. J., Jacob, D. J., Chin, M. & Martin, R. V. Sources of carbonaceous aerosols over the United States and implications for natural visibility. *Journal of Geophysical Research-Atmospheres* **108**, 4355, doi:10.1029/2002jd003190 (2003).
- 67 Fairlie, T. D. *et al.* Impact of mineral dust on nitrate, sulfate, and ozone in transpacific Asian pollution plumes. *Atmospheric Chemistry and Physics* **10**, 3999-4012, doi:10.5194/acp-10-3999-2010 (2010).
- 68 Zender, C. S., Bian, H. S. & Newman, D. Mineral Dust Entrainment and Deposition (DEAD) model: Description and 1990s dust climatology. *Journal of Geophysical Research-Atmospheres* **108**, 4416, doi:10.1029/2002jd002775 (2003).
- 69 Jaeglé, L., Quinn, P. K., Bates, T. S., Alexander, B. & Lin, J. T. Global distribution of sea salt aerosols: new constraints from in situ and remote sensing observations. *Atmospheric Chemistry and Physics* **11**, 3137-3157, doi:10.5194/acp-11-3137-2011 (2011).
- 70 Alexander, B. *et al.* Sulfate formation in sea-salt aerosols: Constraints from oxygen isotopes. *Journal of Geophysical Research-Atmospheres* **110**, D10307,

doi:10.1029/2004jd005659 (2005).

- 71 Heald, C. L. *et al.* Contrasting the direct radiative effect and direct radiative forcing of aerosols. *Atmospheric Chemistry and Physics* **14**, 5513-5527 (2014).
- 72 Fountoukis, C. & Nenes, A. ISORROPIA II: a computationally efficient thermodynamic equilibrium model for K⁺-Ca²⁺-Mg²⁺-NH₄⁽⁺⁾-Na⁺-SO₄²⁻-NO₃⁻-Cl⁻-H₂O aerosols. *Atmospheric Chemistry and Physics* **7**, 4639-4659 (2007).
- 73 Liu, H., Jacob, D. J., Bey, I. & Yantosca, R. M. Constraints from ²¹⁰Pb and ⁷Be on wet deposition and transport in a global three-dimensional chemical tracer model driven by assimilated meteorological fields. *Journal of Geophysical Research* **106**, 12109-12112,12128 (2001).
- 74 Wang, Q. *et al.* Sources of carbonaceous aerosols and deposited black carbon in the Arctic in winter-spring: implications for radiative forcing. *Atmospheric Chemistry and Physics* **11**, 12453-12473 (2011).
- 75 Wesely, M. L. PARAMETERIZATION OF SURFACE RESISTANCES TO GASEOUS DRY DEPOSITION IN REGIONAL-SCALE NUMERICAL-MODELS. *Atmospheric Environment* **23**, 1293-1304 (1989).
- 76 Zhang, L., Gong, S., Padro, J. & Barrie, L. A size-segregated particle dry deposition scheme for an atmospheric aerosol module. *Atmospheric Environment* **35**, 549-560 (2001).
- 77 Lin, S.-J. & Rood, R. B. Multidimensional flux-form semi-Lagrangian

- transport schemes. *Monthly Weather Review* **124**, 2046-2070 (1996).
- 78 Rienecker, M. M. *et al.* The GEOS-5 Data Assimilation System—
Documentation of Versions 5.0.1, 5.1.0, and 5.2.0. 118 (2008).
- 79 Holtslag, A. & Boville, B. Local versus nonlocal boundary-layer diffusion in a
global climate model. *J. Climate* **6**, 1825-1842 (1993).
- 80 Lin, J.-T. & McElroy, M. B. Impacts of boundary layer mixing on pollutant
vertical profiles in the lower troposphere: Implications to satellite remote
sensing. *Atmospheric Environment* **44**, 1726-1739,
doi:10.1016/j.atmosenv.2010.02.009 (2010).
- 81 Hu, L. *et al.* Emissions of C6–C8 aromatic compounds in the United States:
Constraints from tall tower and aircraft measurements. *Journal of Geophysical
Research: Atmospheres* **120**, 826-842 (2015).
- 82 Guenther, A. *et al.* The Model of Emissions of Gases and Aerosols from
Nature version 2.1 (MEGAN2. 1): an extended and updated framework for
modeling biogenic emissions. *Geosci. Model Dev.* **5**, 1471-1492,
doi:10.5194/gmd-5-1471-2012 (2012).
- 83 Hudman, R. C. *et al.* Steps towards a mechanistic model of global soil nitric
oxide emissions: implementation and space based-constraints. *Atmospheric
Chemistry and Physics* **12**, 7779-7795, doi:10.5194/acp-12-7779-2012 (2011).
- 84 Price, C. & Rind, D. A simple lightning parameterization for calculating
global lightning distributions. *Journal of Geophysical Research: Atmospheres
(1984–2012)* **97**, 9919-9933 (1992).

- 85 Murray, L. T., Jacob, D. J., Logan, J. A., Hudman, R. C. & Koshak, W. J.
Optimized regional and interannual variability of lightning in a global
chemical transport model constrained by LIS/OTD satellite data. *Journal of
Geophysical Research-Atmospheres* **117**, D20307, doi:10.1029/2012jd017934
(2012).
- 86 Ott, L. E. *et al.* Production of lightning NO(x) and its vertical distribution
calculated from three-dimensional cloud-scale chemical transport model
simulations. *Journal of Geophysical Research-Atmospheres* **115**, D04301,
doi:10.1029/2009jd011880 (2010).
- 87 van der Werf, G. R. *et al.* Global fire emissions and the contribution of
deforestation, savanna, forest, agricultural, and peat fires (1997–2009).
Atmospheric Chemistry and Physics **10**, 11707-11735 (2010).
- 88 Iacono, M. J. *et al.* Radiative forcing by long - lived greenhouse gases:
Calculations with the AER radiative transfer models. *Journal of Geophysical
Research: Atmospheres (1984–2012)* **113** (2008).
- 89 HTAP. Hemispheric transport of air pollution 2010 Part A: Ozone and
particulate matter. (Economic Commission for Europe, Geneva, 2010).
- 90 Dentener, F. *et al.* Emissions of primary aerosol and precursor gases in the
years 2000 and 1750 prescribed data-sets for AeroCom. *Atmospheric
Chemistry and Physics* **6**, 4321-4344 (2006).
- 91 Wiedmann, T., Wilting, H. C., Lenzen, M., Lutter, S. & Palm, V. Quo Vadis
MRIO? Methodological, data and institutional requirements for multi-region

- input–output analysis. *Ecological Economics* **70**, 1937-1945 (2011).
- 92 Tukker, A. & Dietzenbacher, E. GLOBAL MULTIREGIONAL INPUT–
OUTPUT FRAMEWORKS: AN INTRODUCTION AND OUTLOOK.
Economic Systems Research **25**, 1-19 (2013).
- 93 Wang, Q. *et al.* Global budget and radiative forcing of black carbon aerosol:
Constraints from pole-to-pole (HIPPO) observations across the Pacific.
Journal of Geophysical Research: Atmospheres **119**, 195-206,
doi:10.1002/2013jd020824 (2014).
- 94 Lu, Z. *et al.* Light Absorption Properties and Radiative Effects of Primary
Organic Aerosol Emissions. *Environmental Science & Technology* **49**, 4868-
4877, doi:10.1021/acs.est.5b00211 (2015).
- 95 Myhre, G. *et al.* Radiative forcing of the direct aerosol effect from AeroCom
Phase II simulations. *Atmospheric Chemistry and Physics* **13**, 1853-1877
(2013).
- 96 Paulot, F. *et al.* Ammonia emissions in the United States, European Union,
and China derived by high - resolution inversion of ammonium wet deposition
data: Interpretation with a new agricultural emissions inventory
(MASAGE_NH3). *J. Geophys. Res.* **119**, 4343-4364 (2014).
- 97 EPA. The 2008 National Emissions Inventory (NEI), release v3. (2013).
- 98 Huang, X. *et al.* A high - resolution ammonia emission inventory in China.
Global Biogeochemical Cycles **26**, GB1030, doi:10.1029/2011GB004161
(2012).

- 99 EMEP. EMEP/CEIP 2014 Present state of emission data. (2014).
- 100 Environmental-Canada. The National Pollutant Release Inventory (NPRI). (2015).
- 101 JRC/PBL. Emission Database for Global Atmospheric Research (EDGAR), release EDGARv4.2 FT2010. (2013).

Correspondence:

To whom correspondence and requests for materials should be addressed: Jintai Lin (linjt@pku.edu.cn), Qiang Zhang (qiangzhang@mail.tsinghua.edu.cn), or Yi Huang (yi.huang@mcgill.ca).

Acknowledgments:

This research is supported by the National Natural Science Foundation of China (41422502 and 41175127), the 973 program (2014CB441303), and World Wide Fund for Nature (WWF; 10002399). Zifeng Lu and David Streets at the Argonne National Laboratory acknowledge the support by the Modeling, Analysis and Predictability (MAP) program of the National Aeronautics and Space Administration (NASA) under Proposal No. 08-MAP-0143.

Author contributions:

J. L., Q. Z. and Y. H. conceived the research. D. T., D. P., H. Z., T. F., Z. L., D. S. and Q. Z. calculated the emissions. R. N., Y. Y. and J. L. conducted chemical transport model simulations. X. T., R. N., Y. H. and J. L. conducted radiative transfer

model simulations. J. L., S. D., Y. H. and R. N. led the analysis and writing. All authors contributed to the writing.

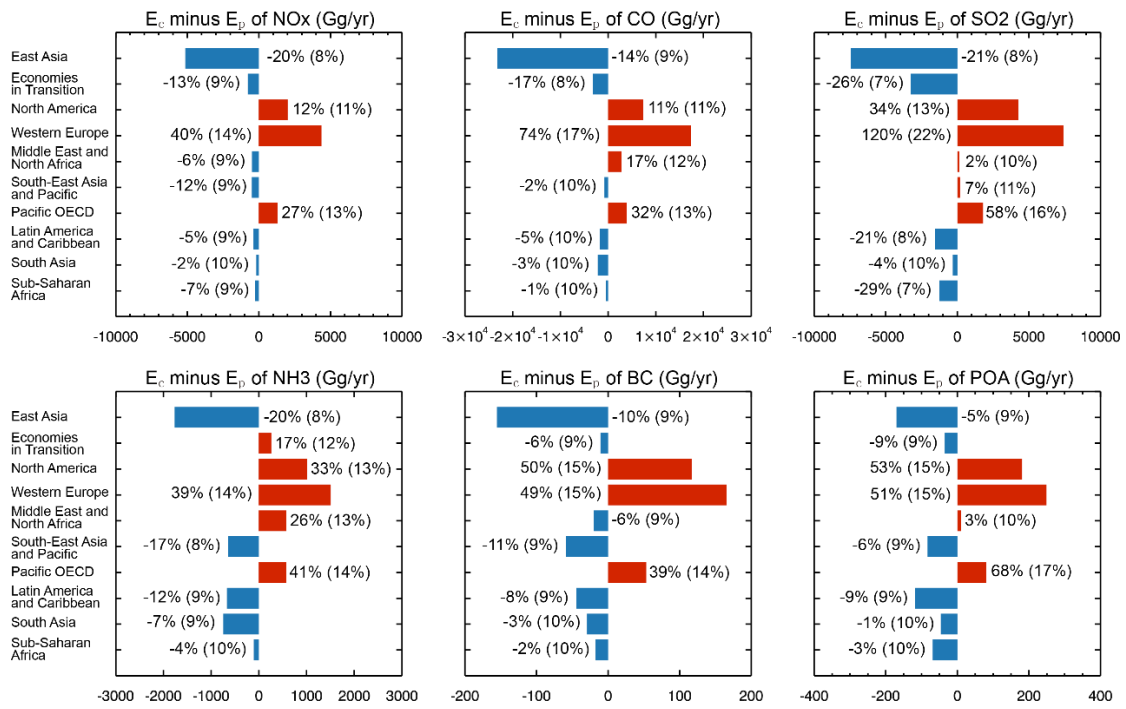


Figure 1 | Net aerosol emissions embodied in trade. $E_c - E_p$ for 10 regions and six aerosol-related species; the values for Rest of the World (including Greenland and the Antarctic) are negligible and omitted here. For a given region, the percentage value indicates the relative change from E_p to E_c , and the value in the parenthesis is the associated error (2σ). East Asia is the largest exporter, and its E_c is lower than E_p by about 20% for NO_x , SO_2 and NH_3 . Western Europe and North America are the largest importers, and their E_c exceeds E_p by up to a factor of 2.

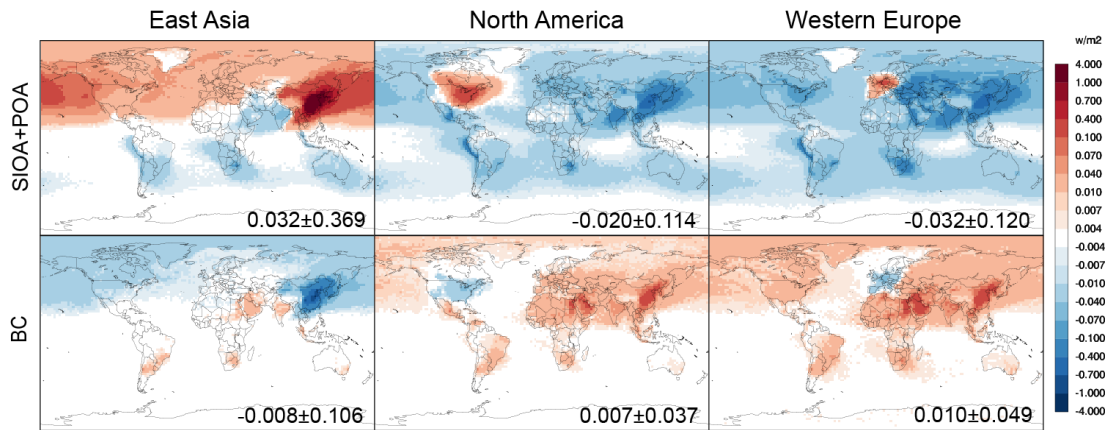


Figure 2 | Global differences between consumption- and production-based radiative forcing ($RF_c - RF_p$). The three columns refer to RF contributed by East Asia, North America and Western Europe, respectively. Given the cooling effect of SIOA+POA, red colors in panels of the first row indicate areas where consumption-based forcing is less negative than production-based forcing. In the case of North America and Western Europe, production-based forcing is relatively confined in space, and consumption-based cooling dominates over most of the globe (blue colors). In contrast, production-based forcing of East Asia's SIOA+POA dominates over most of the Northern Hemisphere. For BC (second row), where the radiative forcing of emissions is positive, the same patterns are visible but with an opposite sign. For each panel, the global mean value is smaller than the standard deviation by a factor of 4–13, highlighting the drastic spatial inhomogeneity of the radiative forcing embodied in trade.

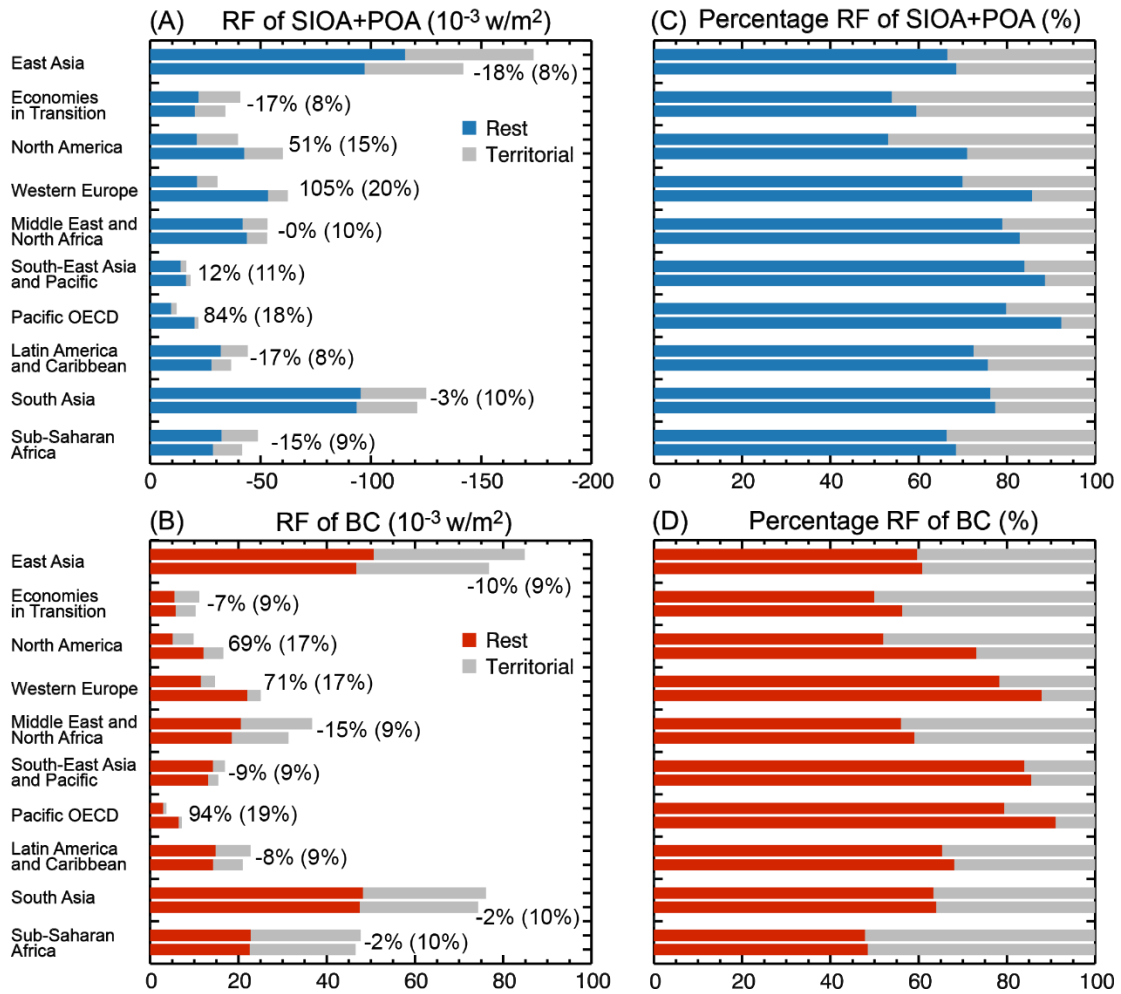


Figure 3 | Global production- and consumption-based radiative forcing of

SIOA+POC and BC for all regions except Rest of the World. (a and b) RF_p

(upper bar) and RF_c (lower bar) contributed by individual regions, summed from the

RF imposed above (grey) and outside (blue in **a** and red in **b**) their territories. For a

given region, the percentage value indicates the relative change from RF_p to RF_c, and

the value in the parenthesis is the associated error (2σ). East Asia, South Asia and

Sub-Sahara Africa produce the strongest RF_c and RF_p, but their RF_c is weaker than

RF_p, particularly for East Asia, the largest exporter. Western Europe and North

America have much stronger RF_c than RF_p, reflecting their outsourcing production to

East Asia and other developing regions. (**c and d**) Similar to (**a and b**) but

highlighting the percentages of RF imposed above (grey) and outside (blue in **c** and red in **d**) the territory of a given region. For each of Western Europe and North America, the percentage of RF imposed above its territory is reduced from RF_p to RF_c by a factor of 2.

Extended Data

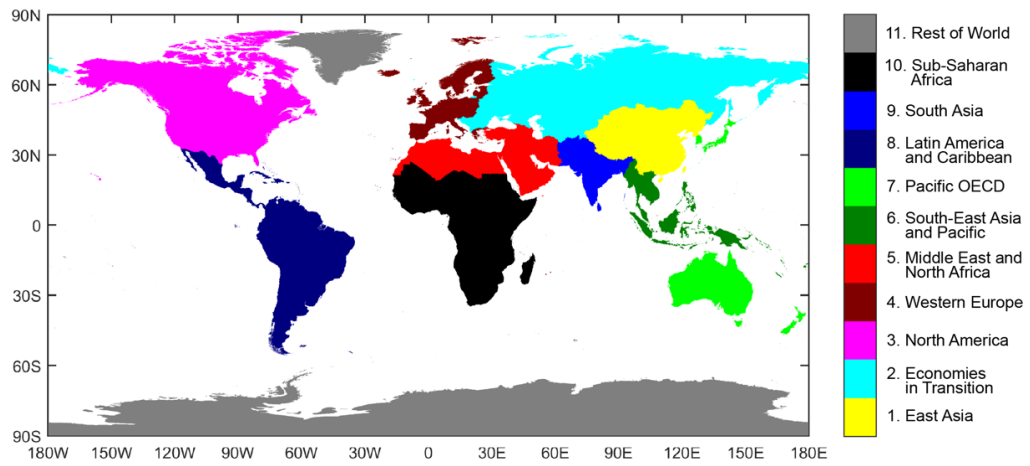
Lin et al.

Extended Data Table 1 | Global RF of SIOA, POC and BC. Radiative forcing of aerosols calculated from three methods: excluding global anthropogenic emissions (with respect to cases R2–R4 for SIOA, POC and BC, respectively, first row), excluding production-based anthropogenic emissions of the 11 regions one by one (cases R5–R37, second row), and excluding consumption-based anthropogenic emissions of the 11 regions one by one (cases R38–R70, third row).

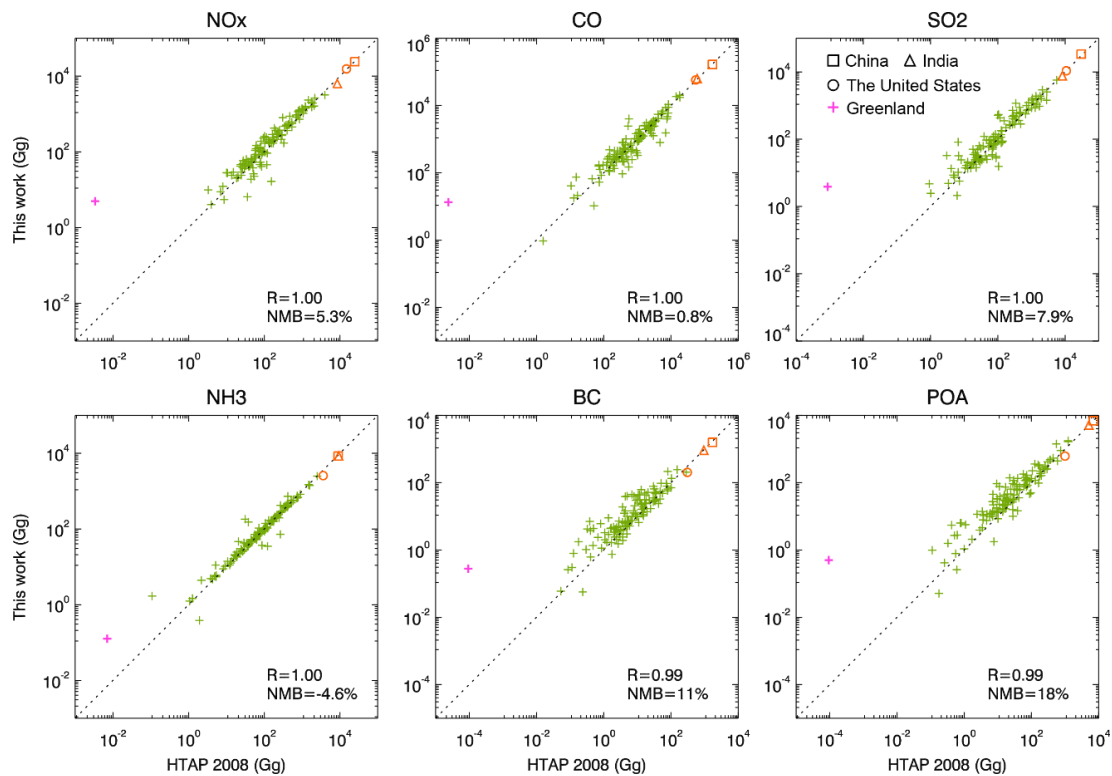
	SIOA	POC	BC
All	-0.481	-0.0990	0.326
Production	-0.486	-0.0984	0.324
Consumption	-0.492	-0.0984	0.324

Extended Data Table 2 | Emission Inventories used in this study for NH₃

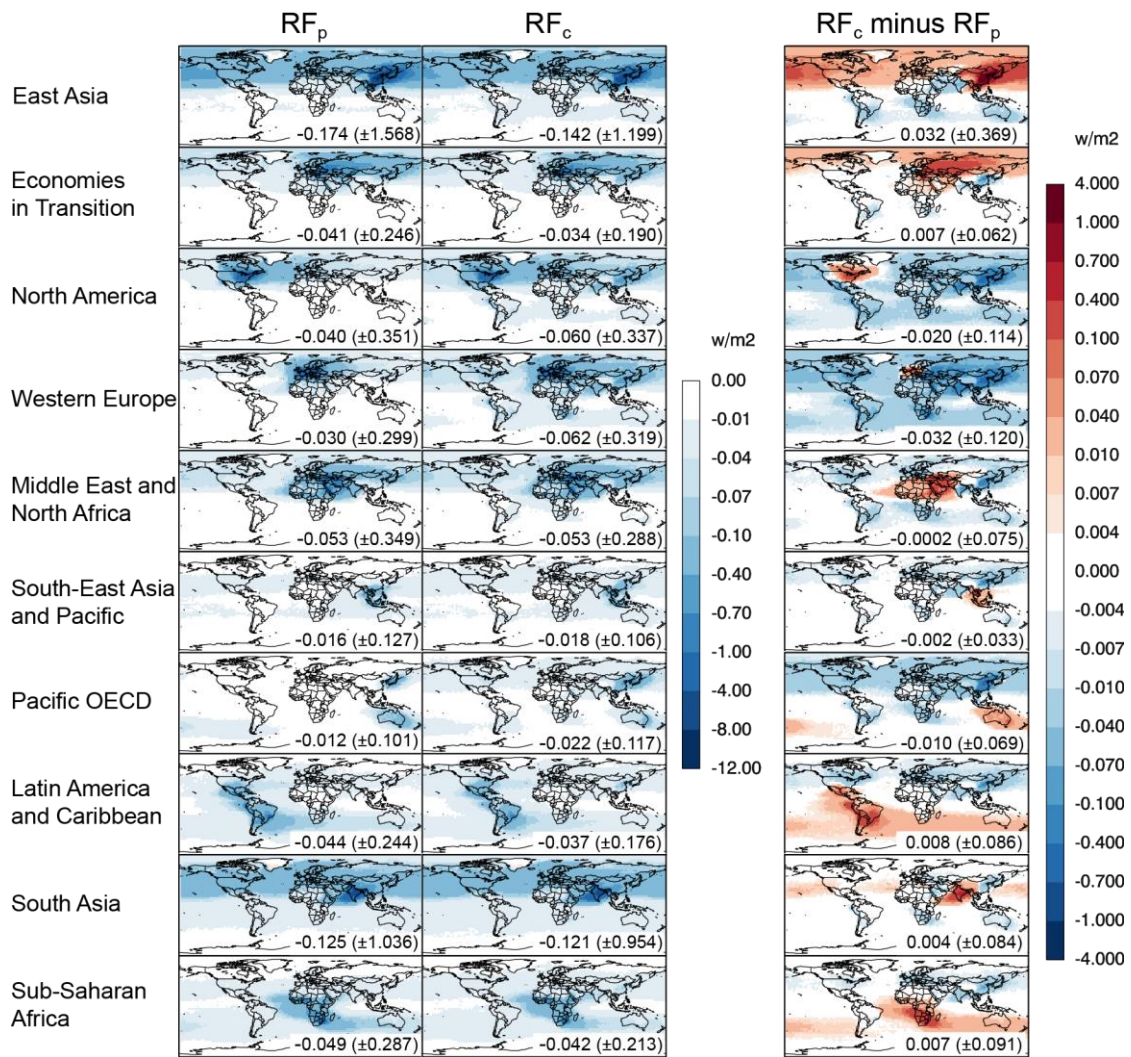
Region	Agriculture (number of sectors)	Other activities (number of sectors)
Contiguous United States	MASAGE (27), ref ⁹⁶	NEI (53), ref ⁹⁷
China	MASAGE (27), ref ⁹⁶	Huang et al. (5), ref ⁹⁸
Europe	EMEP (19), ref ⁹⁹	EMEP (93), ref ⁹⁹
Rest of Asia	REAS (1), ref ⁵⁰	REAS (19), ref ⁵⁰
Canada	NPRI (4), ref ¹⁰⁰	NPRI (113), ref ¹⁰⁰
Other regions	EDGAR (3), ref ¹⁰¹	EDGAR (17), ref ¹⁰¹



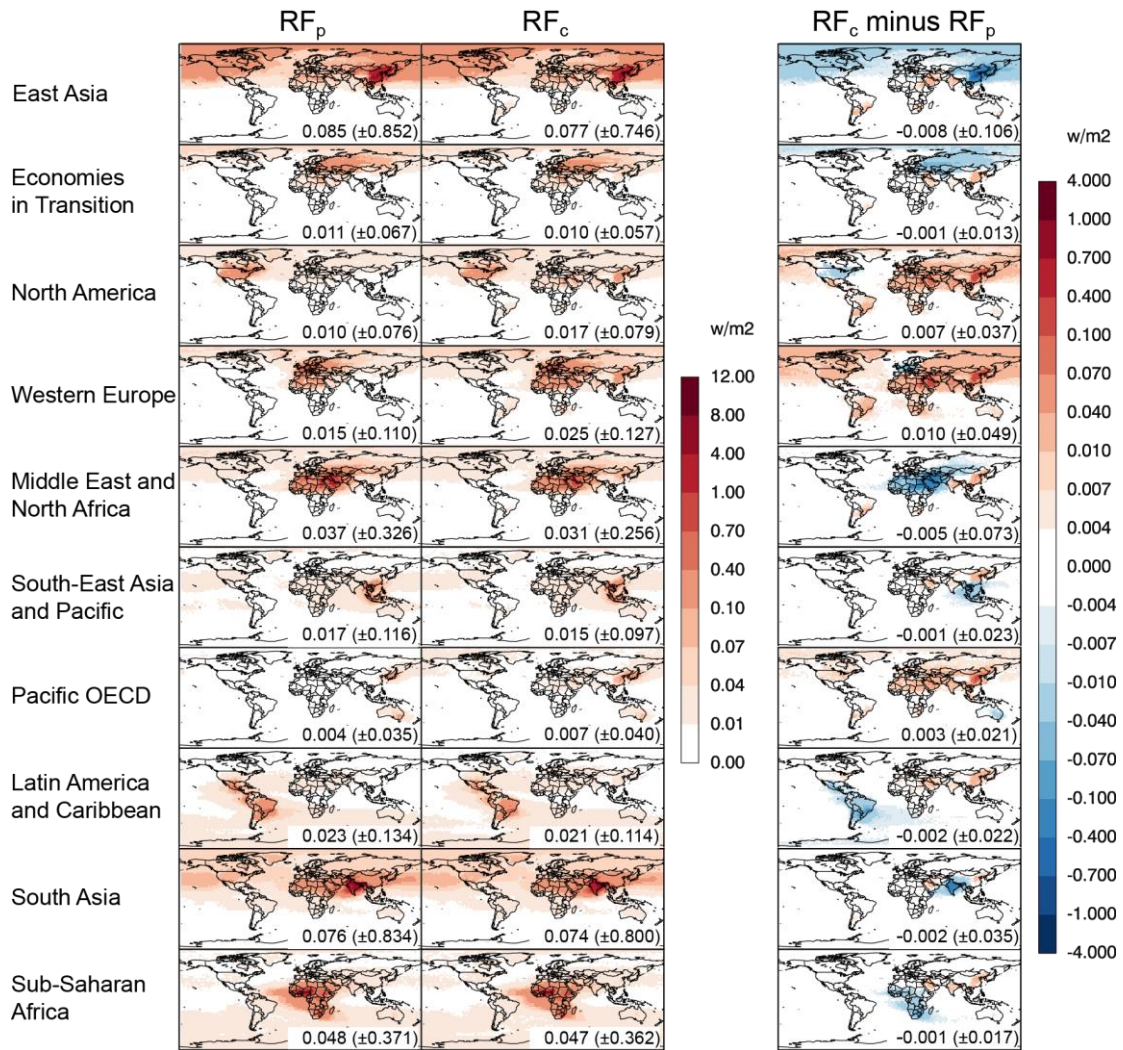
Extended Data Figure 1 | Map of 11 key regions analyzed here. The definition of the first 10 regions follows the IPCC AR5 Working Group 3 Report Chapter 14¹⁶, except that South Korea is included in the Pacific OECD region instead of East Asia region.



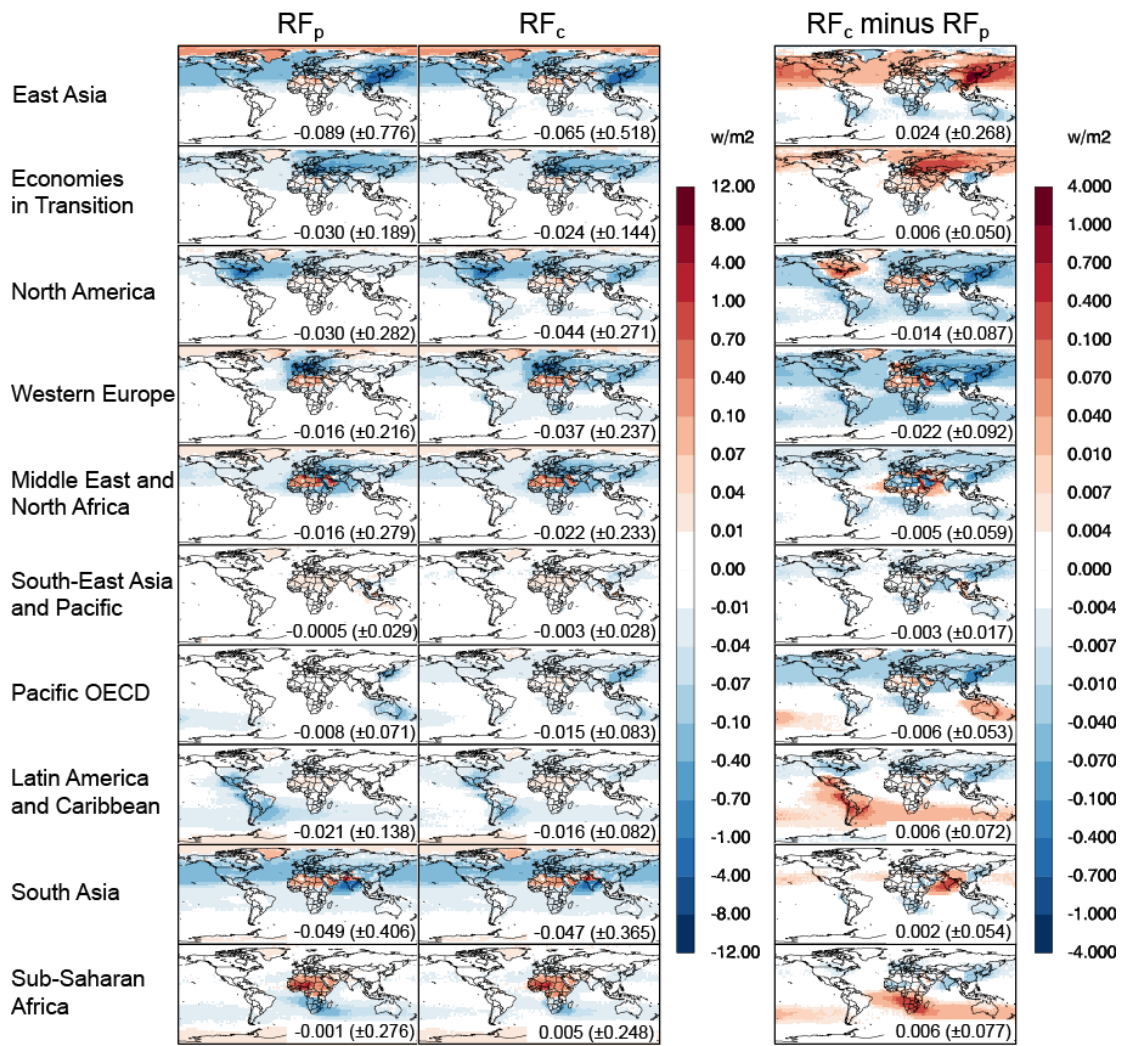
Extended Data Figure 2 | Scatterplot for E_p between this work and the HTAP v2 inventory for 2008. Data are displayed in logarithmic scale for better illustration of small values. In each panel, the correlation (r) and normalized mean bias are also given. The three largest emitters, China, India and the United States, are indicated by special symbols. The outlier region shown in the left of each panel, Greenland, has much higher E_p here than in HTAP v2, although the values are very small in both inventories; the difference is because the IEA fuel database for Greenland used in HTAP v2 contains missing values for fossil fuels, which issue is corrected here by taking the EIA data.



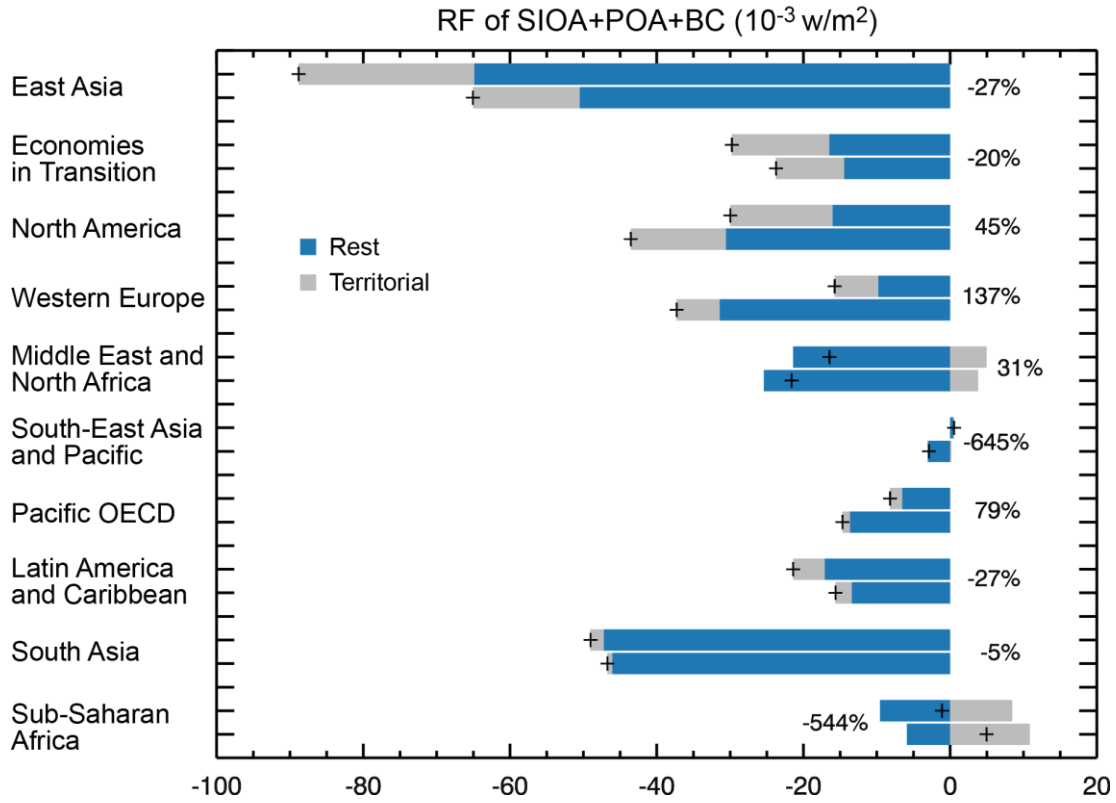
Extended Data Figure 3 | Spatial distribution of production- and consumption-based radiative forcing and their difference for SIOA+POA contributed by individual regions. The numbers in each panel indicate the spatial mean and standard deviation. The color scales are consistent in Extended Data Figs. 3-5.



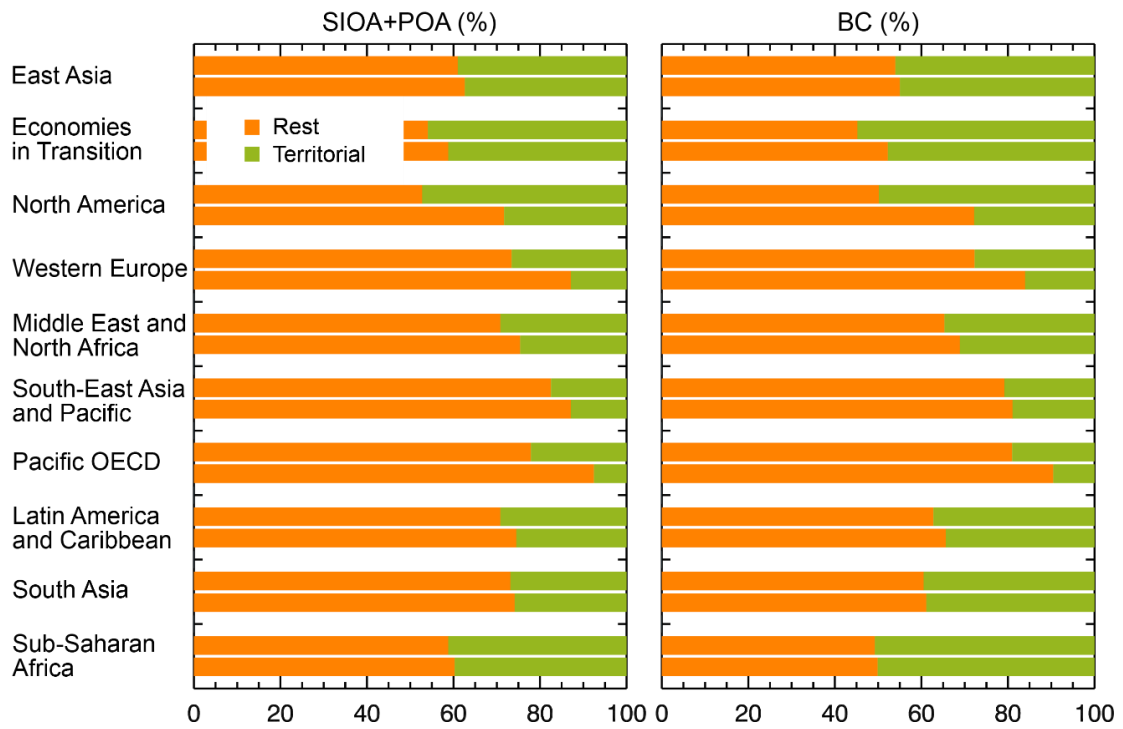
Extended Data Figure 4 | Spatial distribution of production- and consumption-based radiative forcing and their difference for BC contributed by individual regions. The numbers in each panel indicate the spatial mean and standard deviation. The color scales are consistent in Extended Data Figs. 3-5.



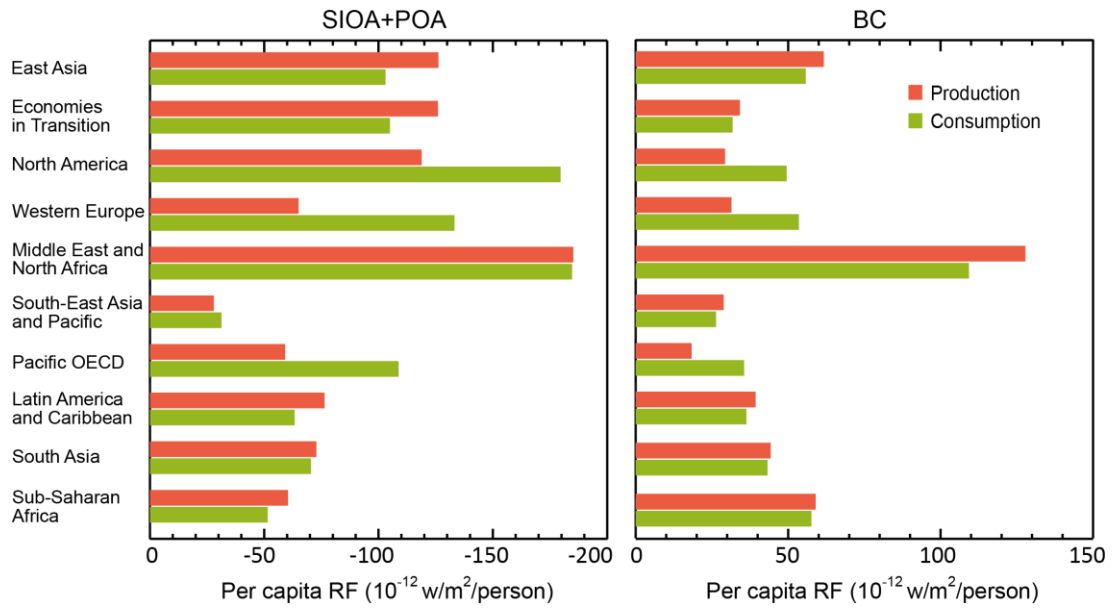
Extended Data Figure 5 | Spatial distribution of production- and consumption-based radiative forcing and their difference for SIOA+POA+BC contributed by individual regions. The numbers in each panel indicate the spatial mean and standard deviation. The color scales are consistent in Extended Data Figs. 3-5.



Extended Data Figure 6 | Global production- and consumption-based radiative forcing of SIOA+POC+BC for the 11 regions. Net RF_p (upper bar) and RF_c (lower bar) of SIOA+POA+BC contributed by individual regions ('+' symbol), summed from the RF imposed above (grey bar) and outside (blue bar) their territories. For a given region, the percentage value indicates the relative change from RF_p to RF_c . For South-East Asia and Pacific, the RF_p imposed outside that region is positive; and the RF_p above that region is close to zero and invisible from the figure. For Sub-Saharan Africa, the RF_c imposed outside that region is negative, but it is more than offset by the positive RF_c imposed above that region.



Extended Data Figure 7 | Percentage fraction of aerosol mass within and outside each region. For the global aerosol mass related to a given region's production (upper bar) or consumption (lower bar), the percentages of aerosol mass above (green bar) and outside (orange bar) the given region.



Extended Data Figure 8 | Production- and consumption-based radiative forcing of SIOA+POC and BC on a per capita basis.